Long-period seismic events with strikingly regular temporal patterns on Katla volcano's south flank (Iceland)

Giulia Sgattoni[1,2,3*], Zeinab Jeddi[3,4], Ólafur Gudmundsson[3], Páll Einarsson[2], Ari Tryggvason[3], Björn Lund[3], Federico Lucchi[1]

[1] *Department of Biological, Geological and Environmental Sciences, University of Bologna, Bologna, Italy*

[2] *Institute of Earth Sciences, Science Institute, University of Iceland, Reykjavik, Iceland*

[3] *Department of Earth Sciences, Uppsala University, Uppsala, Sweden*

[4] *CNDS, Center for Natural Disaster Science, Uppsala University, Uppsala, Sweden*

**Corresponding author:* giulia.sgattoni2@unibo.it

Abstract

Katla is a threatening volcano in Iceland, partly covered by the Mýrdalsjökull ice cap. The volcano has a large caldera with several active geothermal areas. A peculiar cluster of long-period seismic events started on Katla's south flank in July 2011, during an unrest episode in the caldera that culminated in a glacier outburst. The seismic events were tightly clustered at shallow depth in the Gvendarfell area, 4 km south of the caldera, under a small glacier stream at the southern margin of Mýrdalsjökull. No seismic events were known to have occurred in this area before. The most striking feature of this seismic cluster is its temporal pattern, characterized by regular intervals between repeating seismic events, modulated by a seasonal variation. Remarkable is also the stability of both the time and waveform features over a long time period, around 3.5 years. We have not found any comparable examples in the literature. Both volcanic and glacial processes can produce similar waveforms and therefore have to be considered as potential seismic sources. Discerning between these two causes is critical for monitoring glacier-clad volcanoes and has been controversial at Katla. For this new seismic cluster on the south flank we regard volcano-related processes as more likely than glacial ones for the following reasons: 1) the seismic activity started during an unrest episode involving sudden melting of the glacier and a jökulhlaup; 2) the glacier stream is small and stagnant; 3) the seismicity remains regular and stable for years; 4) there is no apparent correlation with short-term weather changes, such as rain storms. We suggest that a small, shallow hydrothermal system was activated on Katla's south flank in 2011, either by a minor magmatic injection or by changes of permeability in a local crack system.

Keywords: Katla volcano, Iceland, long-period earthquakes, volcanic processes, glacial processes

1. Introduction

Katla is one of the most active and threatening volcanoes in Iceland. Partly covered by Mýrdalsjökull glacier (Fig. 1), its volcanic activity has been dominated by large explosive phreatomagmatic eruptions, the latest occurring in 1918. The current repose time is the longest known in history (Larsen, 2000). Katla is located just east of Eyjafjallajökull (Fig. 1) and the two volcanoes appear to be tectonically connected (Einarsson and Brandsdóttir, 2000). Katla is known to have erupted in close succession following its neighbour a few times in recent history (1100 years, Einarsson and Hjartardóttir, 2015). For this reason, the 2010 Eyjafjallajökull eruption prompted scientists' concerns about a possible imminent Katla's eruption and the seismic network around the volcano was densified.

Seismic events at volcanoes are highly variable in terms of waveforms and temporal sequence evolution. Different classification schemes are found in the literature. Some of these schemes are based on local experience, e.g., Minakami (1974) for Japanese volcanoes. Others are more general and try to relate the appearance of the seismograms to the process generating the seismic waves (McNutt, 2005; Chouet, 1996). In several instances it can be verified that the appearance of the seismograms is the result of path effects rather than the source process (Soosalu et al., 2006). A commonly used classification separates the seismic events into LP, VT events, and hybrid or mixed events (McNutt, 2005). Long-period (LP) events are devoid of high frequency in their frequency spectrum, have an emergent P-wave and unclear S-wave. Sometimes the S-wave is missing. Volcano-tectonic (VT) events have the appearance of ordinary tectonic earthquakes, have a broad spectrum, sharp P-wave onsets and a clear S-wave. They are usually attributed to rock failure under crustal stress produced by the activity of the volcano. Hybrid events have characteristics in between the LP and VT events. LP events are of particular interest as they often accompany or precede volcanic eruptions (Chouet, 2003; McNutt, 2005). They can be related to a number of different magmatic and hydrothermal processes, usually

76 associated with fluid movements inside the volcano. Recent studies offer new modelling of LP
77 events as slow-rupture failure in unconsolidated volcanic materials (Bean et al., 2014).

78 As Katla is largely covered by the Mýrdalsjökull glacier, extending over a ~600 km^2 area
79 and entirely covering the summit caldera, direct field studies are not feasible. Thus, indirect
80 methods such as seismic data analysis are important when studying and monitoring the volcano.
81 Katla offers a wide variety of seismic signals to obtain insight into the volcano's internal
82 dynamics. In this respect, it is an unusual volcano in Iceland because of its anomalously high and
83 persistent seismicity (even during volcanic quiescence) despite its tectonic location, outside the
84 main deformation zones (see a further discussion of Katla's tectonic setting in the following
85 section). The only other Icelandic volcanoes comparable to Katla with respect to intense
86 seismicity are located along the plate boundaries (for example Hengill and Bárðarbunga
87 volcanoes; Einarsson, 1991; Jakobsdóttir, 2008).

88 The seismic activity at Katla has primarily been recorded in two distinct source areas (e.g.
89 Einarsson and Brandsdóttir, 2000; Soosalu et al., 2006; Sturkell et al., 2010): i) within the
90 summit caldera and ii) in a region in western Mýrdalsjökull named Goðabunga (Fig. 1). In July
91 2011, though, this general pattern changed. An increase in seismicity and a 23 hour tremor burst
92 were recorded on July 8-9, 2011, associated with deepening of ice cauldrons on the ice cap and
93 flooding from the south-east rim of Mýrdalsjökull glacier that destroyed a bridge on the main
94 road. At the same time, a new cluster of LP seismic events was detected on the south flank, just
95 west of the Gvendarfell Rise (GR – see Fig. 2), around 4 km south of the caldera rim. Seismic
96 events in this area of Katla had never been recorded before and they are of major interest when
97 assessing Katla's volcanic hazard, as the coastal area south of Katla is a farming area and a
98 popular tourist destination.

99 At subglacial volcanoes, seismic events associated with glacier dynamics (such as basal
100 slip, ice falls, crevassing) often lack high frequencies and are sometimes called low-frequency

(LF) events (Métaxian et al., 2003; West et al., 2010; Thelen et al., 2013). Glacial LF events and shallow LP earthquakes associated with volcanic activity can produce similar waveforms and the ability to distinguish between them is critical for monitoring glacier-covered volcanoes. In this respect, Katla aroused controversial interpretations of its seismicity, for its subglacial location and for the unusually frequent occurrence of LP seismicity during periods of volcanic quiescence (Soosalu et al., 2006; Jónsdóttir et al., 2009).

Although the LP events located on Katla's south flank in some aspects resemble those of other volcanoes, they show some peculiar characteristics, especially in their time evolution, which we have not found described in the literature. These are the subjects of our study. The improved seismic network operating around Katla during 2011-2013 provided a good dataset for this purpose. Moreover, in order to improve the location estimates of these events further, a temporal deployment of three stations was done in 2014 in the epicentral area, in order to better define the absolute location of the cluster. We used cross-correlation methods to improve the event detection, thus highlighting striking time-sequence features, and a probabilistic non-linear method for the absolute location of the cluster. We also attempted to retrieve focal mechanisms from first motion polarities.

2. Study area

The Katla volcanic system is located just south of the intersection between the Eastern Volcanic Zone and the transform boundary of the South Iceland Seismic Zone (Fig. 1). It consists of a central volcano with a 110 km^2 summit caldera (up to 14-km wide; Fig. 1) covered by Mýrdalsjökull glacier (Björnsson et al., 2000) and the Eldgjá fissure system which extends 75 km to the northeast (Larsen, 2000; Thordarson et al., 2001; Fig. 1). The central volcano's activity is dominated by explosive phreatomagmatic eruptions due to magma-ice interaction. Several ice cauldrons (at least 16) are located within and at the caldera rim, representing the surface

126 expression of subglacial geothermal activity. Changes in their geometry are monitored to detect
127 variations of geothermal heat release (Guðmundsson et al., 2007).

128 Seismic undershooting within the Katla caldera has revealed a zone where P wave
129 velocities are reduced and through which shear waves do not propagate; this anomaly is
130 interpreted as evidence of a magma chamber (Guðmundsson et al., 1994). Moreover, results from
131 an aeromagnetic survey indicate the presence of a non-magnetic body within the region of the
132 postulated magma chamber (Jónsson and Kristjánsson, 2000). This is supported by geobarometry
133 analyses on historical tephra samples, conducted by Budd et al. (2016), but questioned by tephra
134 stratigraphy studies by Óladóttir et al. (2008).

135 Since the first sensitive seismographs were installed (in the 1960s), seismic activity has
136 been observed in two distinct main areas (Fig. 1): within the caldera and at Goðabunga on the
137 western flank (Einarsson and Brandsdóttir, 2000). The seismicity inside the caldera consists of
138 VT and hybrid events, probably associated with the subglacial geothermal activity (Sturkell et
139 al., 2010) and volcano-tectonic processes. The Goðabunga cluster consists mainly of LP shallow
140 events and has a controversial interpretation, as a response to a slowly-rising viscous cryptodome
141 (Soosalu et al., 2006) or in association with ice fall events (Jónsdóttir et al., 2009). Katla's
142 seismicity shows a seasonal variation which is stronger at Goðabunga, where the peak occurs in
143 autumn. A less pronounced peak of activity in the caldera occurs instead during the summer
144 (July/August; Jónsdóttir et al., 2007). This seasonal correlation has been interpreted either as a
145 result of ice-load change and resulting pore-pressure change at the base of the glacier (Einarsson
146 and Bransdóttir, 2000) or as enhanced glacial motion during periods of distributed subglacial
147 water channels (Jónsdóttir et al., 2009).

148 Although no visible eruptions have occurred after 1918, evidence of unrest was observed
149 in 1955, 1999 and 2011, possibly associated with minor subglacial eruptions. In 1955 this
150 probably took place at the eastern rim of the caldera: two shallow ice-cauldrons formed and a

small jökulhlaup (glacial flood) drained from Kötlujökull, south-east Mýrdalsjökull (Fig. 2; Thorarinsson, 1975; Rist, 1967). A similar event took place in July 1999: the seismic stations around the glacier recorded earthquakes and bursts of tremor that culminated in the release of a jökulhlaup from Sólheimajökull, south-west Mýrdalsjökull (Sigurðsson et al., 2000; Roberts et al., 2003). A new cauldron also formed on the surface of the glacier (Guðmundsson et al., 2007).

From 1999 to 2004, GPS measurements on nunataks (exposed rock protruding through the ice) exposed on the caldera edge revealed steady uplift of the volcano, interpreted to result from 0.01 km^3 magma accumulation (Sturkell et al., 2006; 2008). A recent study by Spaans et al. (2015), suggested instead that the uplift may be due to glacial isostatic adjustment as a consequence of mass loss of Iceland's ice caps.

Guðmundsson et al. (2007) showed that increased geothermal heat output occurred in 2001-2003, based on the evolution of ice cauldrons. As this was also accompanied by greatly increased seismicity and ground uplift, they interpreted these phenomena as a result of magma accumulation and consequent dilation of the edifice leading to enhanced permeability and increased geothermal activity, in accordance with Sturkell et al. (2006).

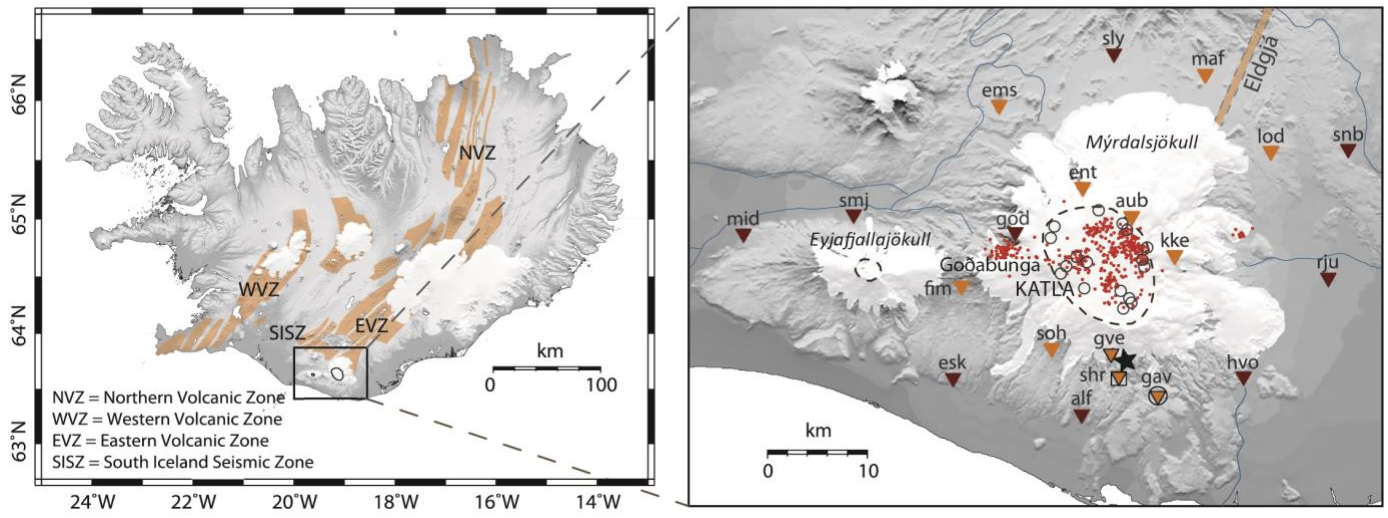

SIZE: 2 columns

Fig. 1. Map of Iceland showing the different volcanic systems (in orange; from Einarsson and Sæmundsson, 1987) and the different segments of the plate boundary. In the inset, the seismic network and main seismic and geological features of Katla are shown. Dark brown inverted triangles: permanent IMO seismic stations. Orange inverted triangles: temporary Uppsala University seismic stations operating between July 2011-August 2013 (no outline) and between July 2014-August 2014 (black outline). The black open circle around the inverted triangle marks a temporary station (GAV) that has been operating on both time periods. The square around the inverted triangle at station SHR on the south flank indicates the location of a GPS station operating between July 2014-August 2014. Red dots: seismic clusters at Katla before July 2011. These are mostly localized in two distinct source areas, within the caldera and on the western flank at Goðabunga. The star marks the new cluster on the south flank. The Katla and Eyjafjallajökull caldera rims are outlined by dashed lines. Open circles correspond to ice cauldrons (Guðmundsson et al., 2007). White areas are glaciers. To the NE, the location of the Eldgjá fissure is shown. Topographic information from National Land Survey of Iceland.

3. The unrest episode of July 2011

Between August 2010 and July 2011, most of the ice cauldrons on the Mýrdalsjökull glacier uplifted by 6-8 m, interpreted by Guðmundsson and Sólnes (2013) as a consequence of water accumulation under the glacier. The greatest rise, 11-12 m was observed at cauldron 16 (Fig. 2; Guðmundsson and Sólnes, 2013).

In July 2011, the seismicity intensified at Katla and remained high until winter. The unrest culminated on July 8-9th when a burst of tremor was recorded by the Icelandic Meteorological Office (IMO) seismic network. No signs of eruption breaking the ice were seen, but a jökulhlaup drained from Kötlujökull and deepening of some ice cauldrons was observed on the surface of Mýrdalsjökull in the southern and eastern parts of the caldera (Fig. 2).

The tremor burst lasted for about 23 hours, beginning at about 19:00 GMT on July 8th. The jökulhlaup (~18 million m^3) swept away the bridge over Múlakvísl river around 05:00 GMT on July 9th, one hour after rising water level was detected at the gauging station Léreftshöfuð, located a few km south of Kötlujökull (IMO, 2011) and ~6 km upstream from the bridge (Fig. 2).

Another gauging station, located on the bridge over Múlakvísl river on the main road 1 (Fig. 2), began to show increased conductivity early on July 8th (IMO, 2011). This unrest episode has been interpreted in association with volcanic processes, such as enhanced geothermal activity, shallow magma intrusion or possibly a minor subglacial eruption (Sgattoni et al., 2015).

The earthquake activity accompanying these events was mainly concentrated inside the caldera, mostly in its south-eastern part. The tremor also originated inside the caldera, in a similar location to the earthquakes (Sgattoni et al., 2015). In addition, a new source of seismic events was activated on the south flank, near the Gvendarfell Rise, at the southern edge of Mýrdalsjökull glacier (Hafursárjökull), around 4 km south of the southern caldera rim (Fig. 2).

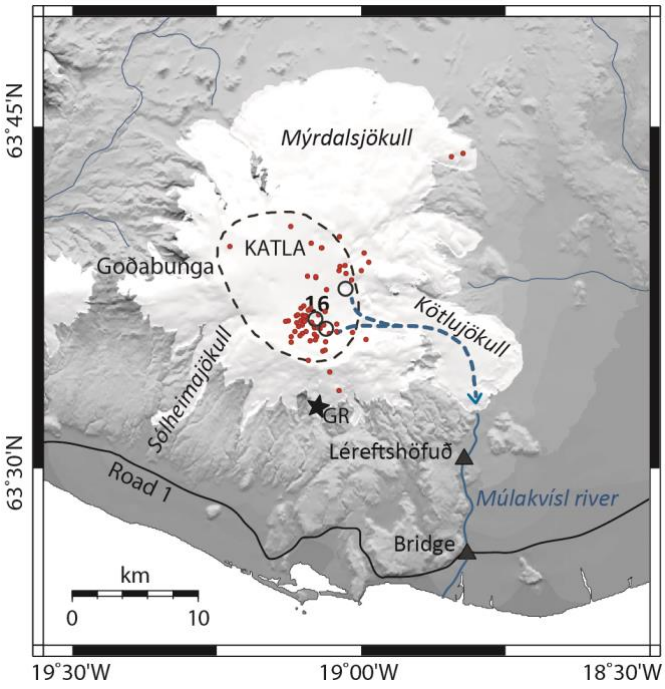

SIZE: 1 column

Fig. 2. Map of Katla showing the features related to the July 2011 unrest. Open circles are the ice cauldrons that deepened during the unrest. Number 16 is the cauldron that showed biggest changes before and during the unrest. The dashed blue arrow shows the presumed flood path. Red dots are the earthquakes that occurred on July 8th and 9th. The two gauging stations are marked with black triangles;

the southern one corresponds to the bridge over Múlakvísl river. The star marks the southern seismic cluster which is studied herein. GR: Gvendarfell Rise. Topographic information from National Land Survey of Iceland.

4. Seismic network and data

Following the eruption of Eyjafjallajökull volcano in 2010, the IMO augmented the seismic monitoring network around Katla from 5 to 9 stations. Moreover, 9 temporary stations were deployed by Uppsala University between July 2011 and August 2013.

Most of the stations were equipped with broadband sensors, 5 Guralp ESPA , 4 Guralp CMG3-ESPC and 1 Geotech KS-2000(LLC), all with flat response from 60 s to the Nyquist frequency (50 Hz). 5-second Lennartz populated the remaining 8 stations. Data were recorded and digitized with Guralp and Reftek systems at 100 sps. Stations were powered with batteries, wind generators and solar panels. All the instruments recorded in continuous mode, but some technical problems (e.g. power failure) mainly due to harsh weather conditions (especially in winter time), prevented some stations from working continuously during the whole operation time.

During the operation time of the dense network described above, the closest station to the Gvendarfell cluster, subject of this study, was GAV, around 6 km away. Therefore, the hypocentral location was poorly constrained, especially in depth (uncertainty on the order of 1 km). Since this seismicity continued with similar characteristics, we decided to install two additional stations, around 1 and 2 km away from the source, during the summer of 2014 to improve the hypocentral location of the cluster. Station GAV was also reoccupied to minimize biases in hypocentral estimations caused by the change in network geometry. In addition, a GPS station was deployed during the same period (Fig. 1).

5. Waveform characteristics

The Gvendarfell seismicity is characterized by small magnitude (~ -0.5-1.2 M_L), long-period earthquakes with an emergent P wave and unclear S wave, which we have confidently identified only at the closest station GVE (Fig. 3). Although a secondary phase is observed on the horizontal components at some other stations (e.g. station ALF; Fig. 3), its arrival times differ on the two components and its particle motion is complex so we do not identify it as an S phase.It is more likely a complex interference pattern of scattered shear waves and surface waves possibly including S-to-P conversions.

All events have remarkably similar, nearly identical waveforms with correlation coefficient ≥ 0.9 at the nearest stations. Fig. 4 shows examples of waveforms throughout the whole time period, starting from March 2011, when the first small events were recorded. The similarity of the waveforms is striking and only slight changes can be noticed, from August 2012. The frequency content is narrow banded around 3-4 Hz at the closest station GVE and nearly monochromatic around 3 Hz at most other stations (Figs. 3 and 4).

The signals are characterized by a number of distinct seismic phases that we tried to interpret with particle motion plots. This however didn't help to discern and understand the different phases, which appear to be generated by interference of direct and scattered waves propagating in a heterogeneous medium. The complexity of the waveforms and their duration are therefore highly dependent on the distance from the source. A 6-7 sec long wave-train recorded at ~1 km distance, becomes more than 20 sec long, at 30-40 km. This is indicative of strong path effects, generating a number of secondary phases that increase the complexity of the seismograms (Fig. 5).

Another interesting feature is that the larger events were often preceded by smaller events, only recorded by the closest station GVE (Fig. 3). At more distant stations, the small events disappear into the background noise.

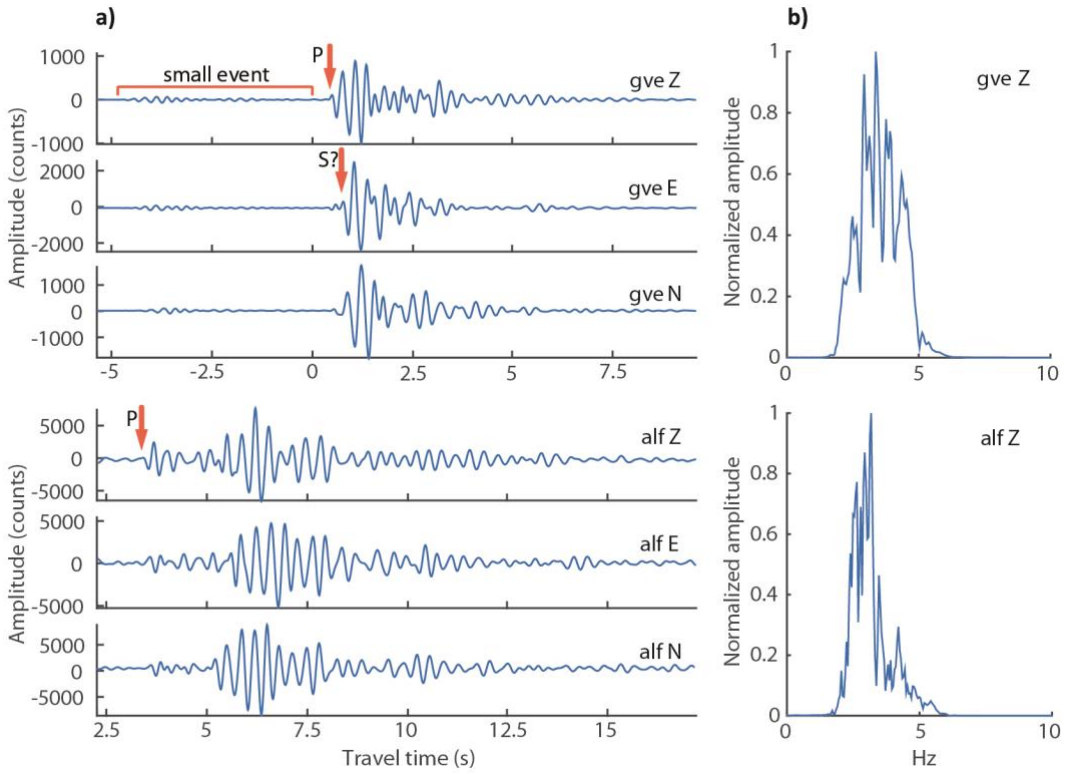

SIZE: 1.5 column

Fig. 3. a) Example seismograms of two different events at stations GVE and ALF. Notice the small event before the main one at GVE. The amplitude unit is digital counts, proportional to velocity. The arrows mark the P and S wave arrivals, where identified. b) Normalised amplitude spectra of the Z component at stations GVE and ALF.

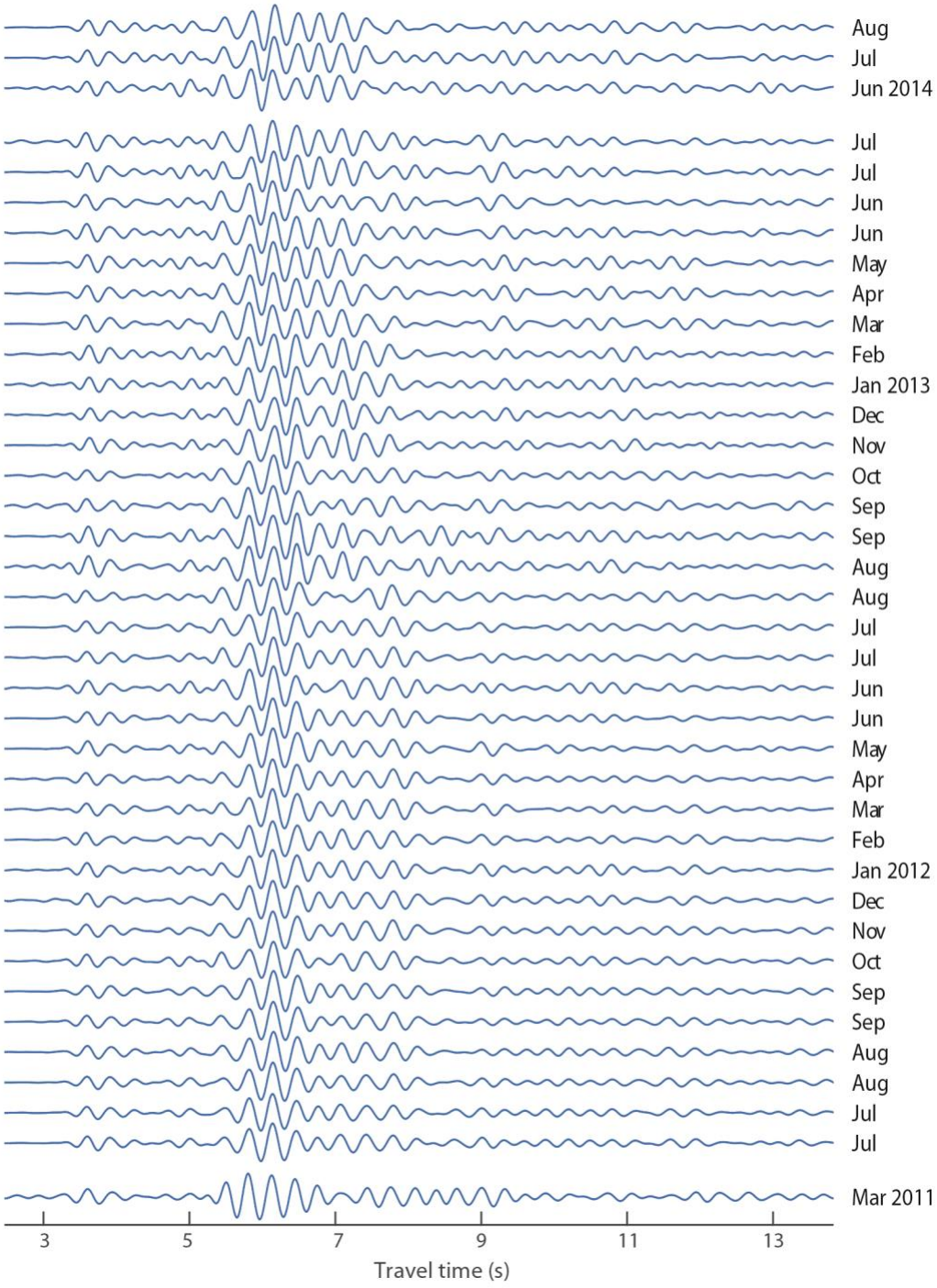

268

269 SIZE: 1.5 column

270 Fig. 4. Example waveforms of the Z component at station ALF (~6 km from the source) throughout the
271 entire period of study, showing their similarity. To avoid cluttering the figure, one event per month is
272 shown for cold seasons (when seismic rate is low) and two events per month for warm seasons (when
273 seismic rate is high).

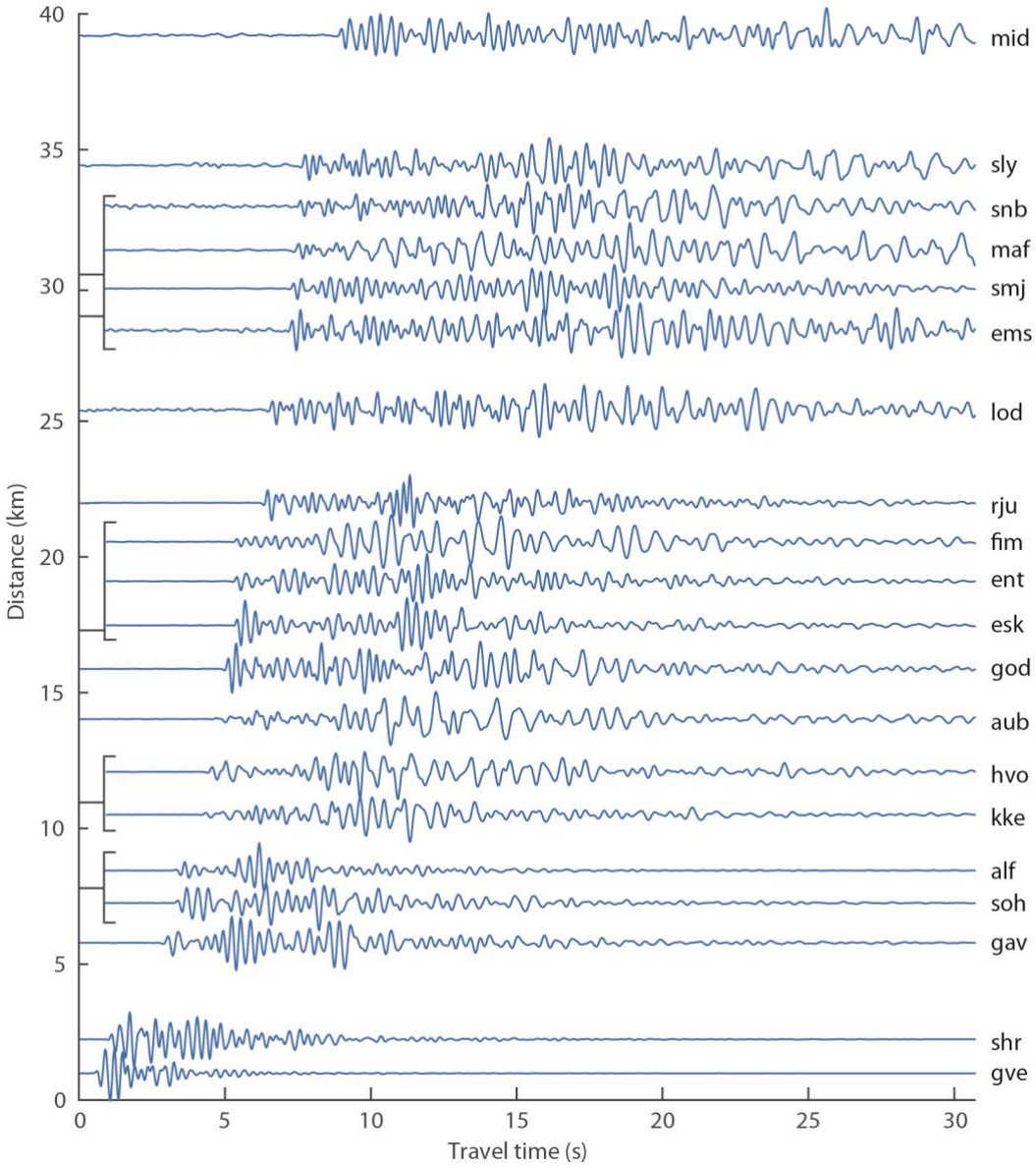

SIZE: 1.5 column

Fig. 5. Stacked Z component seismograms of all events recorded at each station. The approximate epicentral distance is reported on y-axis.

6. Time evolution

Visual observation of the seismic data indicated that a significant improvement in detectability could be achieved, compared with the IMO catalogue. As the waveforms are highly repeatable, cross-correlation of a sample waveform with continuous data was applicable to improve the event detection (cf. Lindblom et al., 2015 for a description of the correlation method). For this purpose we used data from station ALF, as it is close to the source and has been working continuously since February 2011. The best event in terms of signal to noise ratio was chosen from the IMO catalogue as a reference event (occurred on Oct 10, 2011). Its waveform was band-pass filtered between 2-4 Hz and a 3 second window starting 0.5 sec before the P wave arrival was cross-correlated with the continuous data from February 2011 to August 2013. Around 1800 events were detected with a cross-correlation coefficient higher than 0.9 (mostly $\geq$ 0.95), significantly more compared to the 720 events of the IMO catalogue (Fig. 6). All the events were checked for possible false detections and visual inspection of 3 months of data proved that the cross-correlation analysis detected all visible events successfully. Moreover, in order to check whether other similar events had occurred also before 2011, data from station ESK (operating at Katla before the network was augmented) were used for cross-correlation with continuous data from 2010. In this case, no events were detected that matched a minimum correlation coefficient threshold set as 0.7. This confirms that seismic activity at Gvendarfell was absent before 2011.

The local magnitude M_L of the events was evaluated by calibrating the amplitude at ALF with the IMO magnitude estimation (moment magnitude Mw and local magnitude M_L). The events overlapping between our improved catalogue and the IMO catalogue were used as a reference. Fig. 7 shows a logarithmic plot of the maximum amplitude at ALF versus M_L, demonstrating a clear linear relation. A line fitting of the M_L plot was used to translate ALF amplitudes (from our catalogue) into magnitudes (Fig. 7).

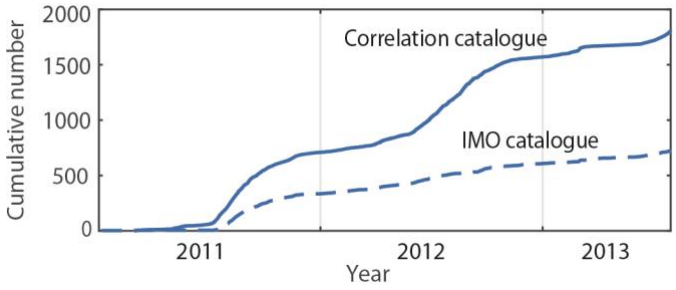

SIZE: 1 column

Fig. 6. Cumulative number of events at Gvendarfell. The event detection of the catalogue obtained with cross-correlation is highly improved. A seasonal variation, with more events during warm seasons (corresponding to the steeper segments of the curve), is also clear on the top curve.

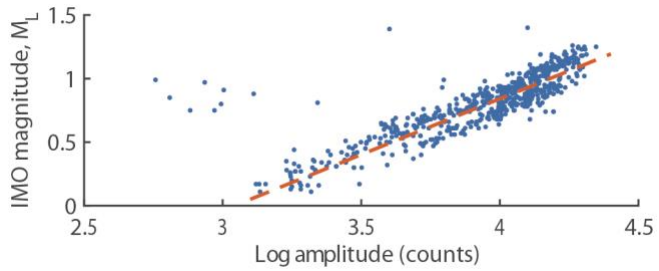

SIZE: 1 column

Fig. 7. Magnitude calibration. The maximum log amplitude at station ALF is plotted for all events of our catalogue overlapping with IMO catalogue. Linear correlation between ALF amplitude and IMO local magnitude, M_L. The dashed line is the line fitted to the data to convert amplitudes to M_L.

The first Gvendarfell events detected at ALF occurred in March 2011 and were very small, around 0.2 M_L (Fig. 8a) A sudden increase in magnitude occurred on July 7th and a striking time feature started on this day: a regular time pattern with 6 events per day at 4 hour intervals began a few hours before the tremor burst of the 2011 unrest episode (Fig. 9). Before that time, this pattern was not observed. A seasonal variation in the event rate is also observed, with maximal activity in late summer 2011, 2012 and 2013, which could not be discerned from the IMO catalogue (Figs. 6, 8a and 9). This correlation is not as clear in the cumulative moment

release plot (Fig. 8b), showing a sharp increase in the summer of 2011 and less clear increases in the following summers. The regular event rate is observed also during periods of lower activity, with occurrence frequency gradually decreasing to 1 event every 1-2 days in winter and then increasing again to the maximum rate (6 to 8 events per day, depending on the year) during summer (Fig. 9). Diurnal variability and correlation with precipitation rates was checked, using weather data from the IMO website. No correlation was found. This pattern is seen for the whole time period analyzed in this article (July 2011-August 2014), although the clearest regularity is observed during the summer of 2011. Some exceptions to this general pattern can be noticed, for example in March 2013 (Fig. 8a), when a small swarm of events was recorded, not correlated with any volcanic/geothermal or meteorological activity. According to the latest data from IMO, the seismic activity at Gvendarfell faded out and became insignificant in February 2015. However, it picked up again by the end of August 2015 and still continues in 2016 with a similar seasonal pattern as before.

The amplitude behavior with time also has interesting features. It increased by a factor of 10 at the onset of the tremor and stayed high for a year (Fig.8). After 1 year, the amplitude decreased by a factor of 2. A non-monotonic size distribution is also observed, with small events occurring in the background, mainly during periods of high seismic activity (Figs. 8a and 9). The regular time pattern is mainly observed for the class of larger events, whereas smaller events seem to occur at more random time intervals (Fig. 9), however this could be due to incompleteness of the catalogue below $M_L = 0$.

Fig. 10 shows the relation between the magnitude and the cumulative number of events. The size of the events does not follow the conventional empirical relation of Gutenberg-Richter ($\log N = a - bM$). The non-monotonic size of the events shows up clearly in the non-cumulative plot in Fig. 10, with a peak around $M_L = 1$ and a minimum around $M_L = 0.4$. Another peak is present at around $M_L = 0$. It is not clear if this is simply caused by incompleteness at magnitudes

< 0 or if this is a feature of the physical distribution. Note that it is impossible to estimate the magnitude of completeness in this case because the earthquakes do not follow any standard model.

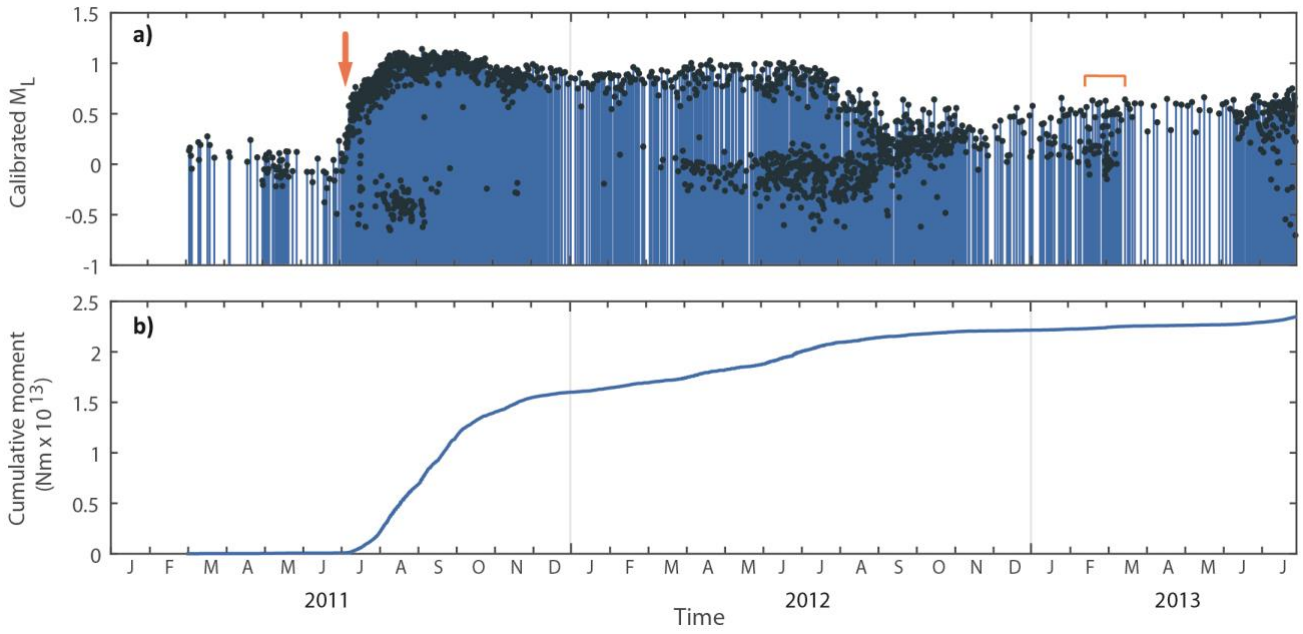

SIZE: 2 columns

Fig. 8. a) Magnitude (M_L) - time evolution of the Gvendarfell seismic sequence between January 2011 and July 2013. The arrow indicates the time of the tremor burst (July 8-9). The March 2013 swarm is also outlined (orange squared line). b) Cumulative seismic moment release in the same time interval as panel (a). The moment-magnitude relation used is $\log M_0 = 1.5M + 9.1$, where M_0 is the moment and M is the magnitude. As we do not have an estimation of Mw, we used M_L in this relation. Therefore, our estimates of seismic moment are uncertain.

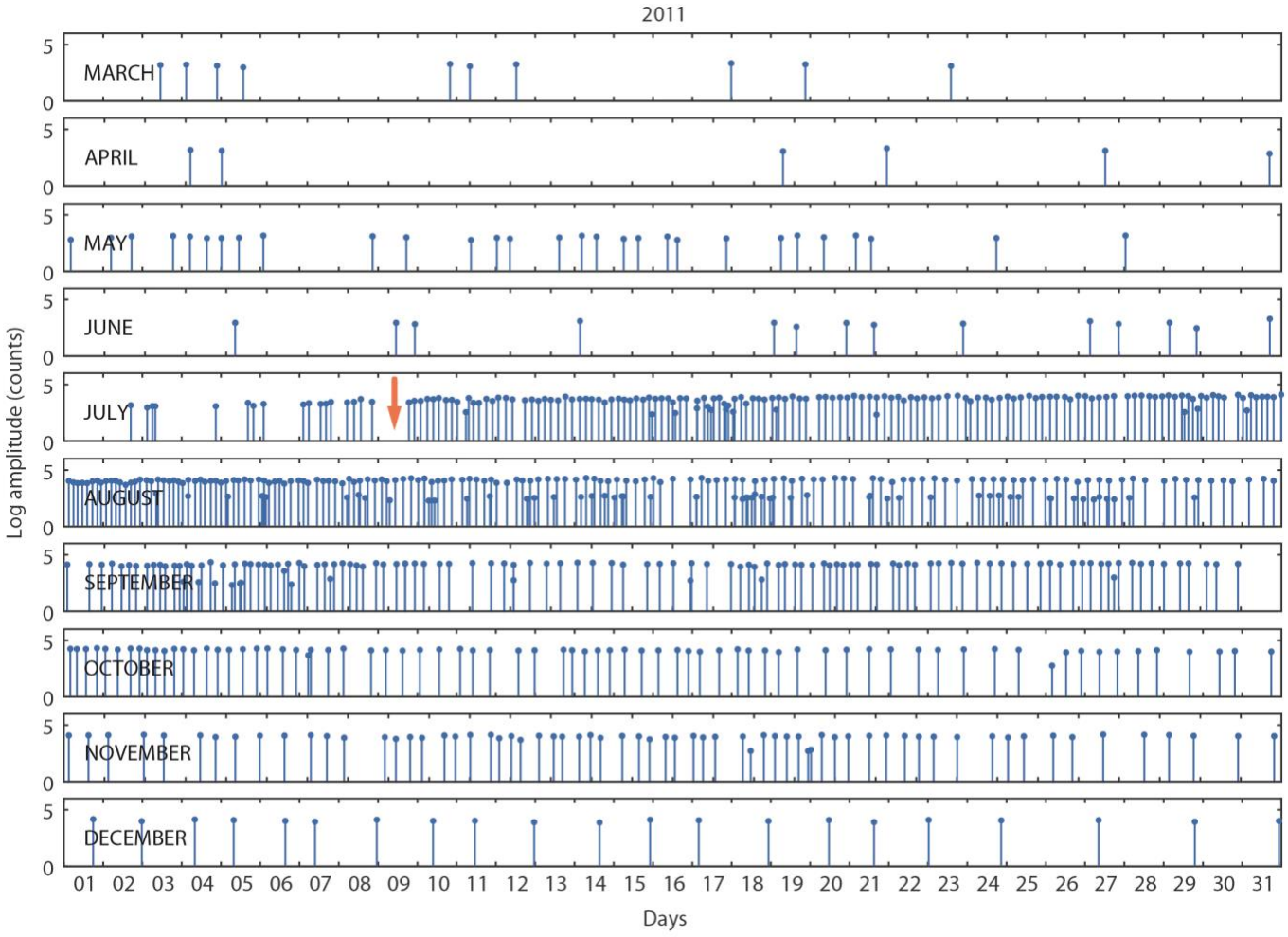

SIZE: 2 columns

Fig. 9. Time evolution of the Gvendarfell seismic sequence in 2011. The arrow indicates the time of the tremor burst, same as Fig. 8, corresponding to the beginning of the regular time pattern. Inter-event times vary between 4 hours in July-August to 1-2 days in December.

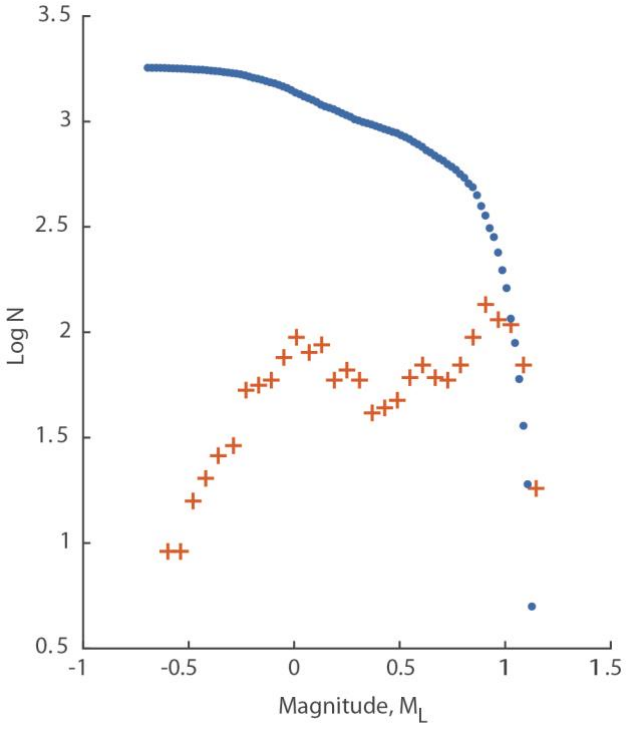

SIZE: 1 column

Fig. 10. Magnitude (M_L) – number (log N) relation, both cumulative (dots) and non-cumulative (crosses).

7. Absolute location

The absolute locations from the IMO catalogue show a cloud of hypocenters, dispersed over a large area, several km in diameter (Fig. 11) around the Hafursárjökull glacial valley, on the southern side of Mýrdalsjökull glacier. However, the similarity of all the waveforms suggests a much smaller distribution of foci, which we can crudely estimate by requiring the phase difference to be smaller than a fraction of a period, in order to explain such high correlation. By taking this fraction as a quarter of a wavelength and assuming a dominant frequency of 3.5 Hz and an average velocity of 3.5 km/s, we can infer the maximum size of the hypocentre distribution to be ≤ 250 m. Reported uncertainty is on the order of 1 km in the horizontal and several km in the vertical, i.e. smaller than the distribution of locations, suggesting that

383 significant and variable (because of changes in station geometry) bias due to three-dimensional
384 heterogeneity is present in the locations.

385 **7.1 Non-linear location method**
386

387 We selected the best recorded events during the summer of 2014 (when 2 additional
388 stations were deployed nearby) to be relocated. For this we used a probabilistic, non-linear
389 method, mapping the likelihood function for each event around the center of the IMO location
390 cloud with an exhaustive grid search (Lomax et al., 2000). The error distributions of arrival-time
391 data and their predictions are assumed to be Gaussian. The error is not known. A distance
392 weighting is assigned for stations farther than 3 km from the source to simulate increasing
393 uncertainty with increasing distance. This defines a data covariance matrix, less an unknown
394 scaling. This scaling is estimated based on the residual variance at minimum misfit and thus
395 represents the combined error of observation and prediction. The velocity model used is one
396 dimensional and based on tomographic results in the area (Jeddi et al., submitted for
397 publication). Scalar station corrections (estimated based on time residuals) are introduced to
398 absorb effects of lateral heterogeneity with an iterative procedure, starting from no corrections
399 and iterating until converging to stable corrections.

400 The grid search extended over a 5x5 km^2 area around the average IMO location of the
401 events recorded in 2011-2013, down to 5 km depth, with 50 m resolution in the horizontal
402 directions and 100 m in the vertical. As the phase composition of the wave forms is unclear (as
403 explained above), particular care was taken when picking the P and S arrival times. The P wave
404 was carefully identified first in the stacked wave forms and then consistently in the individual
405 events (details of the stacking are explained below). The S wave was only picked at the closest
406 station, GVE. The iterative process of relocation and station-correction estimation converged at
407 the second iteration. The resulting rms correction was 0.17 sec.

7.2 Location results

Fig. 12 shows the resulting combined probability density of the hypocenter locations. The origin of the coordinate system is the average IMO location (at N63°32.772' and W19°06.588') and depth is referred to the average elevation in the source region (at 800 m.a.s.l.). Our relocations do not differ much from the IMO average, except for a ~500 m shift to the east. The distribution of hypocenters is much smaller than in the IMO catalog locations (Figs. 11 and 12a). The uncertainty of the relocations is around 400 m in the horizontal dimensions and 500-600 m in depth, as inferred from the probability distributions of the locations of single events (Fig. 12b). The cluster appears to be located in the shallow subsurface, between 0.5 and 0.9 km depth. It is clear from comparing Fig. 12a, showing the combined distribution of the cluster, and Fig. 12b, showing the distribution for an individual event, that the cluster distribution is dominated by the uncertainty. Therefore, the cluster may be much smaller in extent than Fig. 12a suggests. The eastward shift of the center of mass of the distribution compared to the average IMO location is marginally resolved. The depth is marginally resolved to differ from zero. A clear correlation (trade off) is persistent between depth and easting. This is controlled by the station geometry, with the nearest station GVE, yielding S picks, a few km to the west-northwest. Some trade off exists between depth and origin time, but inclusion of S picks from station GVE reduces that significantly.

SIZE: 1.5 column

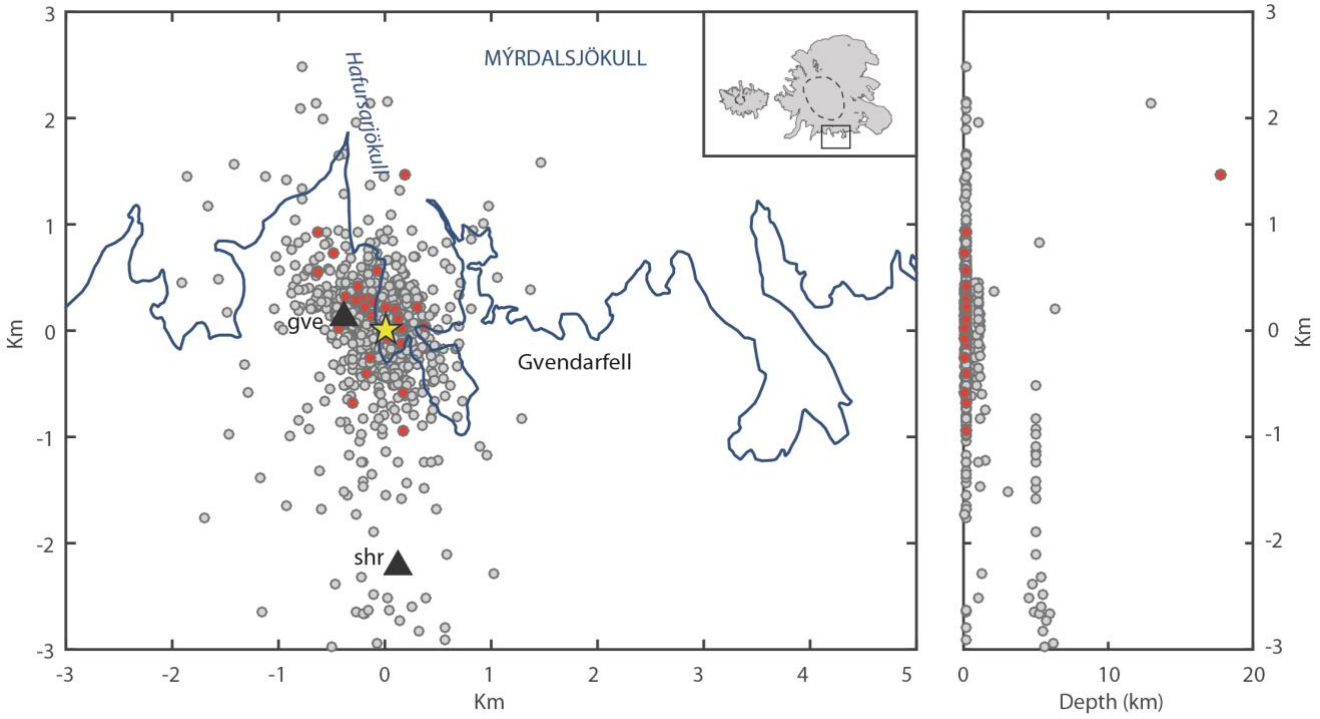

SIZE: 2 columns

Fig. 11. Locations and depth distribution of the Gvendarfell seismic events, from IMO catalogue: grey = all locations 2011-2013; red = 30 events in summer 2014, which are shown relocated with non-linear method in Fig. 12a. The star is the average IMO location (N63°32.772', W19°06.588') and corresponds to the origin of the axes of Fig. 12. Black triangles are the seismic stations. The glacier outline (in blue) is derived from LiDAR DEM obtained in 2010 (Jóhannesson et al., 2013).

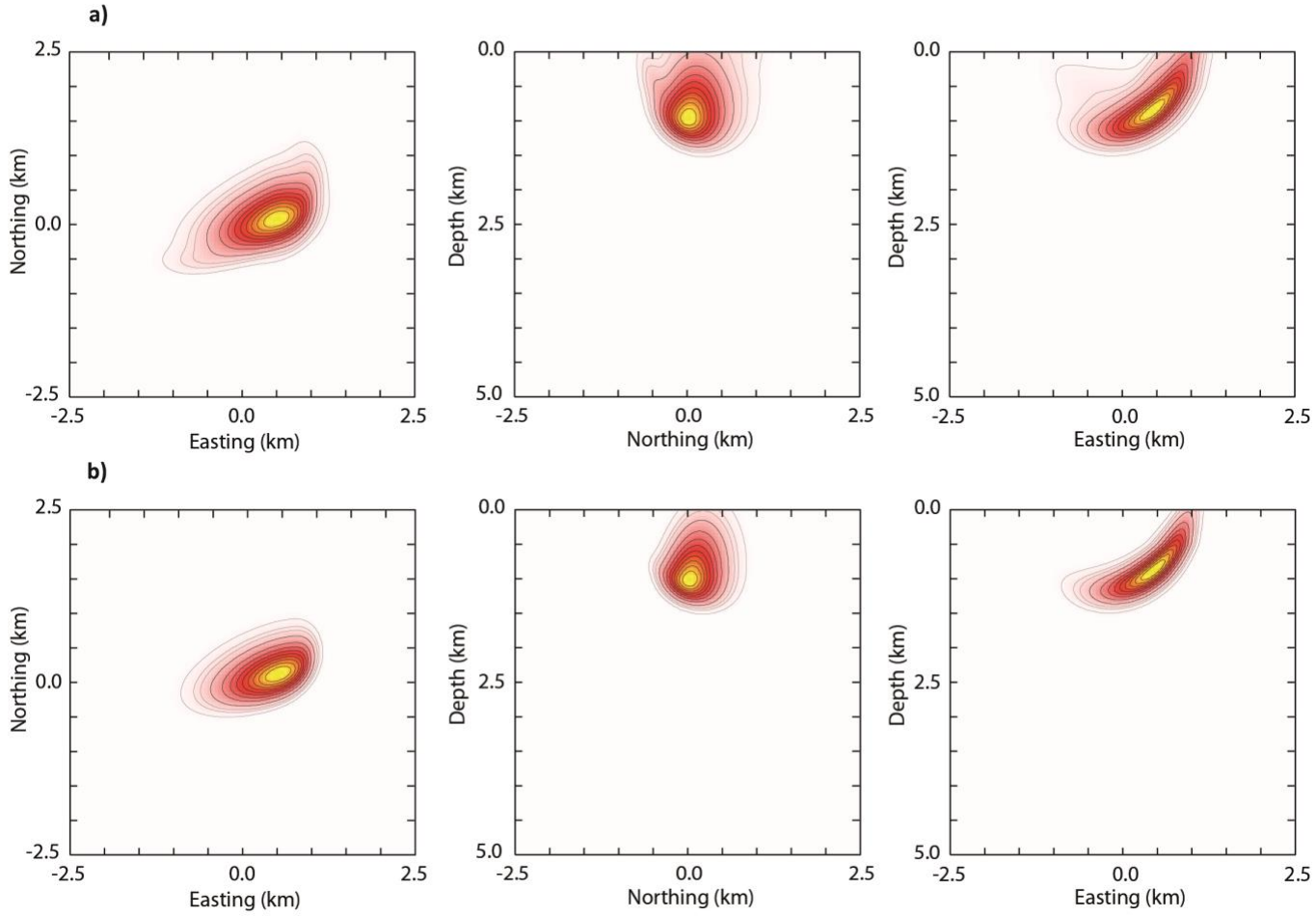

SIZE: 2 columns

Fig. 12. a) Non-linear locations of the Gvendarfell seismic events: combined probability density of all locations (34 events in total occurred in summer 2014). b) Probability density of the location of one example event, to show the single event uncertainty. The scale is normalised and the density ranges from 1 (yellow, in the centre of the distribution) to zero (white). The black contour lines correspond to 0.9 – 0.1 with 0.1 spacing. The grey contour lines are 0.05, 0.03, 0.01.

8. Focal mechanisms

Although we do not know what kind of source generates the Gvendarfell events, we tried to obtain some description of it using regular earthquake source analysis (e.g. focal mechanism

447 based on first motion polarities). If the source is different from that of a tectonic earthquake (e.g.
448 geothermal/volcanic processes involving fluids), a shearing type focal mechanism would be
449 inappropriate, but the first motion descriptions still valuable.

450 The waveforms of the Gvendarfell seismic events are strongly affected by path effects. In
451 addition, the geometry of the network was unfavourable for source studies, with most stations
452 located several kilometers away from the source, mainly because of the glacier. Therefore, it was
453 not considered promising to use a full waveform inversion to constrain the source mechanism.
454 Such a method is also very sensitive to erroneous velocity models, particularly at shallow depth
455 (Bean et al., 2008), which strongly affects stations farther from the source. Therefore, an attempt
456 to retrieve the focal mechanism was done based on the first motion polarities. The emergent P
457 onset is difficult to identify for low-frequency events. Therefore, the signal-to-noise ratio was
458 improved by aligning and stacking all the waveforms at each station (20 stations in total). This
459 was possible thanks to the extreme similarity of the waveforms. Each waveform was weighted
460 according to its signal-to-noise ratio and the uncertainty of the stack evaluated as the variance of
461 the weighted mean.

462 The first arrivals, however, remained unclear at many stations. A closer insight into the
463 zoomed P waves, showed that the first wiggles of all waveforms are highly correlated between
464 different stations. Therefore, by taking the clearest onset (positive polarity at the closest station
465 GVE) as reference, we were able to interpret all the others. We did this by correlating the
466 reference GVE onset with the stacked P onset at all other stations, first the original ones and
467 then the reversed. The stations resulting in the best correlation for the original onset were
468 assigned a positive polarity and vice-versa. The reason for this is intuitive and looks clear from
469 Fig. 13, showing the resulting polarities and the beginning of the seismogram for all stations.

470 The interpretation of the first motions, however, is not trivial and no unique solution of
471 the focal mechanism can be obtained. This arises mainly from the poor coverage of the focal

sphere. Also, as the source is located in the shallow, low-velocity layers, take-off angles can vary considerably and strong scattering effects due to the heterogeneous medium are expected to affect azimuth angles. A tentative fault-plane solution is drawn, consistent with normal faulting. This is however not well constrained and other mechanisms, with different combinations of CLVD (Compensated Linear Vector Dipole) and volumetric components might be invoked. Certainly, the polarities are not consistent with either thrust faulting or with a pure implosion/explosion.

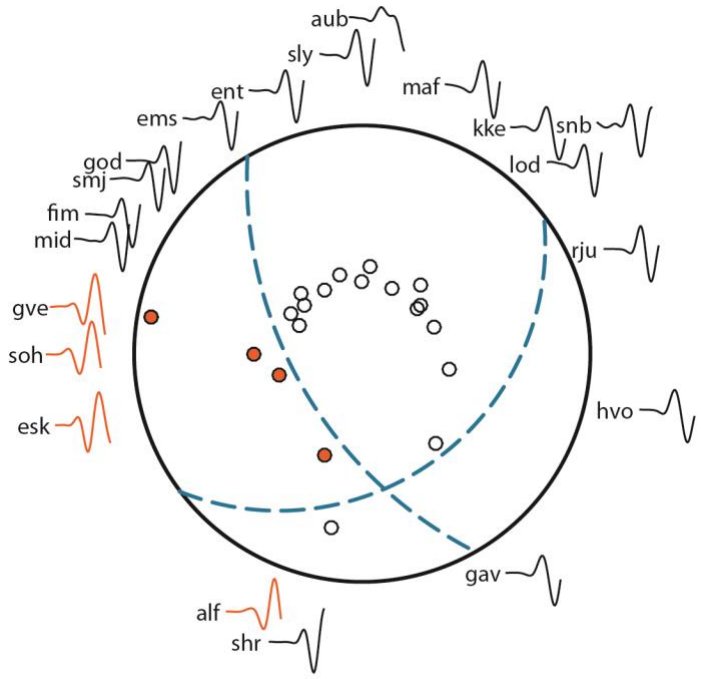

SIZE: 1 column

Fig 13. First motion polarities of the Gvendarfell events, for all seismic stations. Orange dots for positive polarities and white for negative. The beginning of the Z component seismogram for each station is also plotted, with colour corresponding to the polarity. A tentative fault plane solution consistent with normal faulting is drawn.

9. Discussion

9.1 Event classification

The Gvendarfell seismic events have low frequency content, observed at all stations, from the closest (around 1 km) to the farthest (around 40 km). Path effects seem to be important at most stations, as seen from increasing complexity of the waveforms with distance from the source. Moreover, the presence of the glacier might also play a role as a filter for high frequencies (Weaver and Malone, 1979; Métaxian et al., 2003). If this was dominant, we would expect the same effect for the caldera events as well, where the glacier is much thicker, up to 700 m, compared to few tens of meters at Hafursárjökull above the Gvendarfell seismic source. However, we point out that other shallow events originating inside the Katla caldera contain a broader spectrum of frequencies, up to 10-15 Hz, with higher frequencies not completely attenuated by path effects. We therefore interpret the low frequency content of the Gvendarfell events as a source property and classify them as LP events. Moreover, other features of the waveforms are similar to those of LP events at other volcanoes: i) similarity of waveforms, ii) emergent onset of P wave, iii) unclear S wave, iv) narrow peaked spectra with typical frequencies between 0.5 and 5 Hz (Chouet, 2003).

9.2 Glacial vs volcano-related source

As the depth of the cluster is not distinguishable with certainty from the surface and the location corresponds to a glacier stream, glacial processes must be considered also as possible sources of the Gvendarfell seismicity. Glacial earthquakes can be associated with glacier sliding, e.g. stick-slip ice motion (Weaver & Malone, 1979; Ekström et al., 2006; Wiens et al, 2008; Thelen et al., 2013) or with ice avalanches and ice falls (Weaver & Malone, 1979; Caplan-Auerbach and Huggel C., 2007; Roux et al., 2008; Jónsdóttir et al., 2009). Resonance of ice cracks (Métaxian et al., 2003) or resonance of the glacier (Wolf and Davies, 1986) can also generate LP events, but for the reasons discussed below, we consider resonance processes unlikely. A glacial origin of these events could be in accordance with the seasonal variation observed, as it is usual

for glacier seismicity to peak during warm seasons (e.g. Wolf and Davies, 1986; West et al., 2010; Moore et al., 2013). Glacier movements are enhanced due to summer melting, which in Iceland peaks in July and August, after the summer thaw. An example of regular and repetitive glacial seismicity over years has been observed in a Transantartic Mountains glacier (Winberry et al., 2015). The size (likely a few hundred meters) and slip-rate (50 m per year) of that glacier are however much bigger compared to Hafursárjökull glacier. Hafursárjökull is a small, stagnant alpine glacier, not more than few tens of meters thick, and is unlikely to be capable of producing such persistent seismicity. Fig. 14 shows a picture of the glacier, highlighting its small size and showing its actual margin, compared to the outline drawn in Fig. 11. The seismicity of alpine glaciers is usually highly variable in amplitude, recurrence interval, waveforms and often shows changes on diurnal basis and correlation with precipitation rates (Thelen et al., 2013). None of these characteristics are seen at Gvendarfell, where only one family of nearly identical seismic events has been observed for more than 3 years. In addition, if a relation existed between the Gvendarfell seismicity and glacial processes, it would be difficult to understand why similar events are not observed at more active glacier streams nearby or at other glaciers in Iceland. As a final consideration, the time association with the unrest episode in July 2011 seems easier to reconcile with volcanic or geothermal processes.

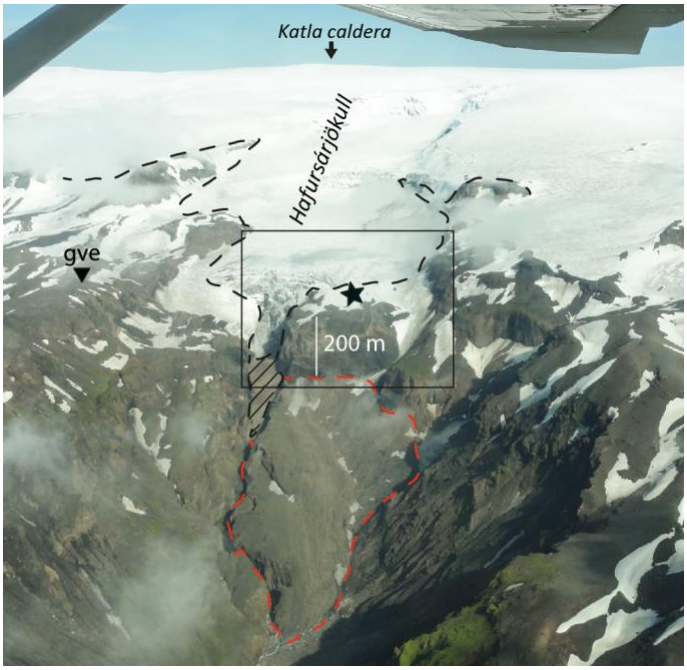

SIZE: 1 column

Fig. 14. Aerial view of Hafursárjökull glacier. The red dashed line is the glacier outline shown in Fig. 11. The black dashed line is the actual glacier limit in August 2015. The area marked with black lines is ice covered by debris. The star corresponds to the approximate location of the center of the absolute hypocenter locations (obtained with the non-linear method, Fig. 12) and the box crudely indicates its uncertainty. The approximate location of the seismic station GVE is also drawn with a black inverted triangle.

9.3 Interpretation of the source process

Due to their association with eruptions, it is commonly thought that LP events are caused by fluid movements within the volcano, for example magma injection into fractures or crypto-dome formation (Okada et al., 1981; Cruz and Chouet, 1997; Rowe et al. 2004; Neuberg et al., 2006), or processes related to hydrothermal systems (Moran et al., 2000; Saccorotti et al., 2007; Guðmundsson and Brandsdóttir, 2010; Jousset et al., 2010; Matoza and Chouet, 2010; Arciniega-Ceballos et al., 2012). The narrow-banded frequency range of LP seismograms at volcanoes is

often associated with resonance processes in which the dominant frequency of the source is related to specific geometries and/or fluid characteristics. In particular, monochromatic, volcanic LP events may be interpreted in terms of resonance of fluid-filled cracks (e.g. Chouet, 1996; Kumagai and Chouet, 1999; Saccorotti et al., 2007). However, a resonance process is expected to generate a long coda of decaying harmonic oscillations, which is not observed in the Gvendarfell events. While most stations record a long-duration signal, resembling resonance, the proximal observation from GVE station is short in duration and indicative of a more pulse-like source rather than resonating. This feature of LP events has been described by Bean et al. (2014) and explained as a strong path effect, very pronounced for shallow sources in the low-velocity, near-surface layers. They carried out a dynamic rupture simulation and showed that long-period signals can be generated by slow-rupture in unconsolidated volcanic materials. This indicates that LP events are not necessarily generated in association with fluid movements.

The high repeatability of waveforms and regular occurrence of LP events characteristic of the Gvendarfell seismicity have been observed at other volcanoes worldwide (Cruz and Chouet, 1997; Ramos et al., 1999; Green and Neuberg, 2006; Rowe et al. 2013), often associated with rising domes (e.g. Okada et al., 1981; Neuberg et al., 2006) or with the interaction of hydrothermal and magmatic systems. For example, repetitive LP events at Popocatépetl were associated with the non-destructive process of repetitive injection of hydrothermal fluid into a fracture resulting in a sudden discharge when a critical pressure is reached (Arciniega-Ceballos et al., 2012). Matoza and Chouet (2010) interpreted repetitive LP events occurring at Mt. St. Helens with regular inter-event time spacing in terms of rapid heating of water and dissolved volatiles in a shallow hydrothermal crack, with events triggered by phase changes from liquid to vapor. In ~~all~~ most cases, repeating LP seismicity has been observed either prior to or during eruptions, their repeatability lasts for days to months and the regular time intervals between successive events are on seconds to minutes scale. The Gvendarfell events, instead, did not

precede or accompany an eruption (at least not in the same area), although they started in coincidence with a tremor event recorded inside the caldera. Moreover, the same waveforms have been recorded for around 3.5 years, occurring with regular inter-event times ranging from hours to days, depending on the season. These features make the Gvendarfell seismicity a unique case.

The Gvendarfell events are also different compared to the other LP events recorded at Katla, most of which are located at Goðabunga, on the western flank of the volcano. The other Katla LP events have a wider spectrum of frequencies, with higher frequencies in the beginning of the waveform decreasing towards the end, as opposed to the nearly monochromatic waveforms at Gvendarfell. In addition, no other cluster at Katla is composed of only one family of waveforms and no other cluster has a similar regular time pattern. The seasonal correlation also differs: the Goðabunga activity peaks later in autumn (Einarsson and Brandsdóttir, 2000; Jónsdóttir et al., 2009) as opposed to July/August at Gvendarfell and the caldera events have a less pronounced seasonality.

The non-monotonic size distribution is also peculiar and is reflected in the magnitude-cumulative number curve, where it is difficult to identify a unique b-value (Fig. 10). Earthquakes below $M_L = 1$ clearly dominate, implying that the source size is restricted and not capable of producing events larger than a threshold size. A similar case, with minor events occurring in the background of larger LP events, was observed at Mt. St. Helens during the 2004-2008 eruption period and interpreted in terms of less energetic fluid to gas phase changes, involving a smaller volume of fluid in a shallow hydrothermal crack (Matoza and Chouet, 2010). Non-linear magnitude-frequency relationships are commonly observed at volcanoes, e.g. the earthquakes accompanying the dyke injection at Krafla in September 1977 (Brandsdóttir and Einarsson, 1979).

Since we could not model the source mechanism, for the reasons discussed in section 8, we are not able to discuss in detail the physical process generating the Gvendarfell events. However,

598 the striking time evolution, together with the repeatability of the waveforms over years, are
599 indicative of a remarkably stable process repeating itself at regular time intervals, modulated by
600 seasons, for an unusually long time. Although glacial processes cannot be completely ruled out,
601 we regard volcano-related processes as more likely to generate such a stable seismicity.

602 Among volcanic processes, both magma-related (e.g. magma intrusion, dome formation)
603 and non-magma related hydrothermal processes (e.g. fluid instabilities, thermal cracking) are
604 candidate sources. The former interpretation fits with the geological evidence of silicic extrusive
605 bodies at the caldera rim and on the eastern and southern flanks of Katla (Lacasse et al., 2007;
606 Jóhannesson and Sæmundsson, 2009). A similar aureole of silicic domes is found around the
607 caldera of Krafla in Northern Volcanic Zone (Jónasson, 1994). Therefore, a rising shallow viscous
608 magma body is a plausible geological processes in the Gvendarfell area. A normal faulting
609 mechanism with a dilatational component, consistent with the first motion polarities shown in
610 Fig. 13, could fit with the hypothesis of an intruding dike. The time association with the tremor
611 episode of the 2011 unrest would also fit with such magma-related interpretation. However, the
612 GPS station operating during the summer of 2014 around 2 km south of the hypocentral area
613 (Fig. 1) did not report evidence of ground deformation to support the hypothesis of a slowly
614 intruding dyke. Moreover, the seasonal correlation of the seismicity appears difficult to reconcile
615 with magma-related processes. Thus, we regard hydrothermal processes as more likely than
616 magma movements to explain this seismicity. A minor hydrothermal system might have been
617 activated on Katla's south flank during the unrest episode in July 2011. The regular time pattern
618 of the seismicity could be associated with a steady process of cyclic heating and cooling of the
619 fluid phase in a hydrothermal crack system with LP events generated by phase changes between
620 liquid and vapor (Matoza and Chouet, 2010). In this scenario, the seasonal correlation of the
621 seismicity could be explained in terms of varying supply of ice melt water to the hydrothermal
622 system, with peaks correlating with the warm seasons. Less energetic phase changes, involving

smaller volumes of fluids, might explain the subset of smaller events. The first motion polarities, although not univocally interpretable, can be consistent with non-double-couple mechanisms observed at other geothermal areas such as Hengill in Iceland (e.g. Miller et al., 1998). However, we point out that there is no visible evidence of geothermal activity, new or old, in the area. The new hydrothermal system, therefore, has to be entirely concealed. Furthermore, a new hydrothermal system needs a new heat source. A small dyke injection into the southern caldera wall or changes to a permeable crack system in conjunction with the thermal event in July 2011 are possible scenarios. A summary of possible interpretations and corresponding pros and cons is reported in Table 1.

Process	Pros	Cons
GLACIAL e.g. glacier sliding, ice-falls	- seasonal correlation - shallow depth	- small, stagnant glacier - no correlation with precipitation rates - association with unrest episode - stability of the process over long time - depth (?)
VOLCANIC (magma involved) e.g. dome rising, viscous magma injection	- geological evidences: silicic extrusive bodies at the caldera rim and south/east flanks - association with unrest episode - normal faulting mechanism (?)	- seasonal correlation - no ground deformation detected
HYDROTHERMAL (no magma involved) e.g. phase changes of the geothermal fluid, thermal	- shallow depth - high repeatability - association with unrest episode - seasonal correlation can be explained	- no evidence of geothermal activity

cracking	- regular time pattern can be explained

Table 1. Summary of pros and cons of the three suggested interpretations of the source process of the Gvendarfell seismic events.

10. Conclusions

Since July 2011 the seismicity pattern at Katla volcano has shown changes: a new cluster of shallow, repeating LP seismic events has been observed on Katla's south flank, at the southern edge of Mýrdalsjökull glacier, 4 km south of the caldera rim. The onset of this seismicity coincided with an unrest episode culminated in a glacial flood from the south-east rim of the glacier, on July 9th, 2011. The seismicity on the south flank had never been observed before and continued for around 3.5 years with the same features.

Since these seismic events are located in a glaciated area, both volcanic and glacial processes must be taken into account as possible sources. Because of the characteristics of the small glacier stream and because of the remarkable stability of the main features of the seismicity over years, we regard volcano-related processes as more likely to generate this seismicity. However, we cannot rule out a glacial source and this study highlights the difficulty and the importance of discriminating glacial and volcanic sources at subglacial volcanoes.

Although they share some common features with LP earthquakes at other volcanoes worldwide, the seismic events we have described represent a peculiar case study because of their temporal behavior and because they did not accompany an eruption. Despite a wide (literature) search, we could not find a similar case in the literature. They also differ significantly from other LP events within Katla.

Among volcano-related processes, we suggest a shallow hydrothermal system is more likely than magma movement to explain this seismicity, mainly because the clear seasonal correlation is easier to reconcile with a process involving water. The extremely regular time pattern over a long time (at least 3.5 years) together with the similarity of all the waveforms, point to a stable, non-destructive source mechanism over time. We regard the regular seismic rate, modulated by seasonality, as the most striking feature of this seismicity. Therefore, we look for a steady source process, in both location and mechanism, in which some critical parameter induces the regular time interval between events. This might be related to a steady process of heating and cooling of a fluid phase, in a geyser-like process. As the fluid phase is supplied by the glacier, a seasonal correlation can be expected as a response to the summer ice melting. Our hypothesis is therefore that a small, shallow hydrothermal system might have been activated on Katla's south flank, in coincidence with the 2011 unrest episode. As a power source, we suggest either a short lived dike intrusion towards the south flank or a crack connection to a heat source established during the unrest. However, no evidence of old or new hydrothermal activity has been seen in the area.

Further studies, such as relative relocation of the hypocenters and further insights into the tremor episode of July 2011, will help interpreting the source processes and volcanological implications of this peculiar cluster of LP events on the south flank of Katla.

Acknowledgements

The authors would like to thank the Icelandic Meteorological Office for access to waveform data and catalogue data of the Gvendarfell events. The temporary deployments producing data for this study were supported by CNDS (Centre for Natural Disaster Science, www.cnds.se) at Uppsala University and the Volcano Anatomy project, financed by the Icelandic Science Foundation. This work was funded by the University of Bologna, University of Iceland and

682 Uppsala University, as a part of a joint PhD project. We thank Heidi Soosalu for the thorough
683 review and valuable suggestions to improve this paper. We thank also the sheriff in Vík for
684 logistic support and Vincent Drouin for the flight over the area. The Generic Mapping Tool was
685 used to produce some of the graphics.

686

687 References

688 Arciniega-Ceballos, A., Dawson, P., Chouet, B. a., 2012. Long period seismic source characterization at
689 Popocatépetl volcano, Mexico. Geophys. Res. Lett. 39, 1–5. doi:10.1029/2012GL053494

690 Bean, C., Lokmer, I., O'Brien, G., 2008. Influence of near-surface volcanic structure on long-period seismic
691 signals and on moment tensor inversions: Simulated examples from Mount Etna. J. Geophys. Res.,
692 113, B08308. doi:10.1029/2007JB005468

693 Bean, C.J., De Barros, L., Lokmer, I., Metaxian, J.P., O'Brien, G., Murphy, S., 2014. Long-period seismicity
694 in the shallow volcanic edifice formed from slow-rupture earthquakes. Nature Geoscience, 7 (1), 71-75.

695 Björnsson, H., Pálsson, F., Guðmundsson, M.T., 2000. Surface and bedrock topography of the Mýrdalsjökull
696 ice cap, Iceland: The Katla caldera, eruption sites and routes of jökulhlaups. Jökull 49, 29-46.

697 Brandsdóttir, B., Einarsson, P., 1979. Seismic activity associated with the September 1977 deflation of the
698 Krafla central volcano in northeastern Iceland. J. Volcanol. Geotherm. Res. 6 (3), 197-212.

699 Budd, D. A., Troll, V. R., Dahren, B., Burchardt, S., 2016. Persistent multitiered magma plumbing beneath
700 Katla volcano, Iceland. Geochem. Geophys. Geosyst. 17, 966–980, doi:10.1002/2015GC006118.

701 Caplan-Auerbach, J., C. Huggel, 2007. Precursory seismicity associated with frequent, large ice
702 avalanches on Iliamna volcano, Alaska. J. Glaciol., 53 (180), 128-140.

703 Chouet, B.A., 1996. Long-period volcano seismicity: its source and use in eruption forecasting. Nature, 380,
704 309-316.

705 Chouet. B.A., 2003. Volcano Seismology. Pure Appl. Geophys. 160, 739-788.

706 Cruz, F.G., Chouet, B.A., 1997. Long-period events, the most characteristic seismicity accompanying the
707 emplacement and extrusion of a lava dome in Galeras Volcano, Colombia, in 1991. J. Volcanol.
708 Geotherm. Res., 77, 121-158.

709 Ekström, G., Nettles, M., Tsai, V. C., 2006. Seasonality and increasing frequency of Greenland glacial
710 earthquakes. Science, 311, 1756– 1758.

711 Einarsson, P., 1991. Earthquakes and present-day tectonism in Iceland. Tectonophysics 189, 261–279.

712 Einarsson, P., Sæmundsson, K., 1987. Earthquake epicenters 1982-1985 and volcanic systems in
713 Iceland. In Þ.I.Sigfússon, ed. *Í hlutarins eðli*, Festschrift for Þorbjörn Sigurgeirsson. Menningarsjóður,
714 Reykjavík (map).

715 Einarsson, P., Brandsdóttir, B., 2000. Earthquakes in the Mýrdalsjökull area, Iceland, 1978–1985:
716 Seasonal correlation and relation to volcanoes. Jökull 49, 59–73.

717 Einarsson, P., Hjartardóttir, Á. R., 2015. Structure and tectonic position of the Eyjafjallajökull volcano, S-
718 Iceland. Jökull 65, 1-16.

719 Green, D.N., Neuberg, J., 2006. Waveform classification of volcanic low-frequency earthquake swarms and
720 its implication at Soufrière Hills Volcano, Montserrat. J. Volcanol. Geotherm. Res. 153, 51–63.
721 doi:10.1007/1-4020-4287-6_4

722 Guðmundsson, Ó., Brandsdóttir, B., 2010. Geothermal noise at Ölkelduháls, SW Iceland. Jökull 60, 89-102.

723 Guðmundsson, Ó., Brandsdóttir, B., Menke, W., Sigvaldason, G.E., 1994. The crustal magma chamber of
724 the Katla volcano in South Iceland revealed by 2-D seismic undershooting. Geophys. J. Int. 119, 277–
725 296.

726 Guðmundsson, M.T., Högnadóttir, Þ., Kristinsson, A.B., Guðbjörnsson, S., 2007. Geothermal activity in the
727 subglacial Katla caldera, Iceland, 1999–2005, studied with radar altimetry. Annals of Glaciology 45,
728 66–72.

729 Guðmundsson, M.T., Sólnes, J., 2013. Activity at Katla and jökulhlaup in Múlakvísl river 2011 (in
730 Icelandic). In: Natural Hazard in Iceland: Volcanic eruptions and earthquakes (in Icelandic. Eds. J.
731 Sólnes, F. Sigmundsson, and B. Bessason). University of Iceland Press, p. 228-229.

IMO, Icelandic Meteorological Office, 2011. http://en.vedur.is/.

Jakobsdóttir, S.S., 2008. Seismicity in Iceland: 1994–2007. Jökull 58, 75–100.

Jeddi, Z., Tryggvason, A., Gudmundsson, Ó., 2016. The Katla volcanic system imaged using local earthquakes recorded with a temporary seismic network, submitted to J. Geophys. Res.

Jóhannesson, T., Björnsson, H., Magnússon, E., Guðmundsson, S., Pálsson, F., Sigurðsson, O., Thorsteinsson, T., Berthier, E., 2013. Ice-volume changes, bias estimation of mass-balance measurements and changes in subglacial lakes derived by lidar mapping of the surface Icelandic glaciers, Ann. Glaciol. 54(63), 63–74. doi:10.3189/2013AoG63A422

Jóhannesson, H., Sæmundsson, K., 2009. Geological Map of Iceland. 1:600.000. Bedrock Geology, 1st edition. Icelandic Institute of Natural History, Reykjavík.

Jónasson, K., 1994. Rhyolite volcanism in the Krafla central volcano, north-east Iceland. Bull. Volcanol. 56, 516-528.

Jónsdóttir, K., Tryggvason, A., Roberts, R., Lund, B., Soosalu, H., Bodvarsson, R., 2007. Habits of a glacier covered volcano: seismicity and a structure study of the Katla volcano, South Iceland. Annals of Glaciology 45, 169–177.

Jónsdóttir, K., Roberts, R., Pohjola, V., Lund, B., Shomlai, Z. H., Tryggvason, A., Bodvarsson, R., 2009. Glacial long-period seismic events at Katla volcano, Iceland. Geophys. Res. Lett. 36, L11402.

Jónsson, G., Kristjánsson, L., 2000. Aeromagnetic measurements over Mýrdalsjökull and vicinity. Jökull 49, 47–58.

Jousset, P., Haberland, C., Bauer, K., Arnason, K., Weber, M., Fabriol, H., 2010. Seismic Tomography and Long-Period Earthquakes Observation and Modelling at the Hengill Geothermal Volcanic Complex , Iceland. Proc. World Geotherm. Congr. 2010 25–29.

Kumagai, H., Chouet, B.A., 1999. The complex frequencies of longperiod seismic events as probes of fluid composition beneath volcanoes. Geophys. J. Int. 138, F7–F12.

Lacasse, C., Sigurðsson, H., Carey, S.N., Jóhannesson, H., Thomas, L.E., Rogers, N.W., 2007. Bimodal volcanism at the Katla subglacial caldera, Iceland: Insight into the geochemistry and petrogenesis of rhyolitic magmas. Bulletin of Volcanology 69, 373–399.

Larsen, G., 2000. Holocene eruptions within the Katla volcanic system, south Iceland: characteristics and environmental impact. Jökull 49, 1–28.

Lindblom, E., Lund, B., Tryggvason, A., Uski, M., Bödvarsson, R., Juhlin, C., Roberts, R., 2015. Microearthquakes illuminate the deep structure of the endglacial Pärvie fault, northern Sweden. Geophys. J. Int., 201, 1704–1716.

Lomax, A., Virieux, J., Volant, P., Berge, C., 2000. Probabilistic earthquake location in 3D and layered models: Introduction of a Metropolis-Gibbs method and comparison with linear locations. In: Thurber, C.H., Rabinowitz, N. (eds.), Advances in Seismic Event Location, Kluwer, Amsterdam, 101-134.

Matoza, R. S., Chouet, B. A., 2010. Subevents of long-period seismicity: Implications for hydrothermal dynamics during the 2004–2008 eruption of Mount St. Helens. J. Geophys. Res., 115, B12206. doi:10.1029/2010JB007839

McNutt, S.R., 2005. Volcanic Seismology, Ann. Rev. Earth Planet. Sci. 33. doi: 10.1146/annurev.earth.33.092203.122459

Métaxian, J.-P., Araujo, S., Mora, M., Lesage P., 2003. Seismicity related to the glacier of Cotopaxi Volcano, Ecuador. Geophys. Res. Lett. 30(9), 1483. doi: 10.1029/2002GL016773

Miller, A.D., Foulger, G.R., Julian, B.R., 1998. Non double-couple earthquakes 2. Observations. Rev. Geophys. 36, 551-568.

Minakami, T., 1974. Seismology of volcanoes in Japan. In: Physical Volcanology (Eds. Civetta, L., Gasparini, P., Luongo, G., and Rapolla, A.), Elsevier, Amsterdam, Oxford, New York, p. 1-27.

Moore, P. L., Winberry, J. P. , Iverson, N. R., Christianson, K. A., Anandakrishnan, S., Jackson, M., Mathison, M. E., Cohen., D., 2013. Glacier slip and seismicity induced by surface melt. Geology, 41(12), 1247-1250.

781 Moran, S.C., Zimbelman, D.R., Malone, S.D., 2000. A model for the magmatic–hydrothermal system at
782 Mount Rainier, Washington, from seismic and geochemical observations. Bull. Volcanol. 61, 425–436.
783 doi:10.1007/PL00008909

784 Neuberg, J. W., Tuffen, H., Collier, L., Green, D., Powell, T., Dingwell, D., 2006. The trigger mechanism of
785 low-frequency earthquakes on Montserrat. J. Volcanol. Geotherm. Res. 153, 37-50.

786 Okada, H., Watanabe, H., Yamashita, H., Yokoyama, I., 1981.Seismological significance of the 1977–1978
787 eruptions and the magma intrusion process of Usu volcano, Hokkaido. J. Volcanol. Geotherm. Res. 9,
788 311 –334.

789 Ramos, E., Hamburger, M.W., Pavlis, G.L., Laguerta, E.P., 1999. The low-frequency earthquake swarms at
790 Mount Pinatubo, Philippines: implication for magma dynamics. J. Volcanol. Geotherm. Res. 92, 295–
791 320.

792 Rist, S., 1967. Jökulhlaups from the ice cover of Mýrdalsjökull on June 25, 1955 and January 20, 1956.
793 Jökull 17, 243–248.

794 Roberts, M. J., Tweed, F. S., Russell, A. J., Knudsen, Ó., Harris, T. D., 2003. Hydrological and geomorphic
795 effects of temporary ice-dammed lake formation during jökulhlaups. Earth Surf. Processes Landforms
796 28, 723– 737.

797 Roux, P. F., Marsan, D., Métaxian, J. P., O'Brien, G., Moreau, L., 2008. Microseismic activity within a serac
798 zone in an alpine glacier. J. Glaciol., 54, 157– 168.

799 Rowe, C.A., Thurber, C.H., White, R.A., 2004. Dome growth behavior at Soufriere Hills Volcano,
800 Montserrat, revealed by relocation of volcanic event swarms, 1995-1996. J. Volcanol. Geotherm.
801 Res.134, 199-221.

802 Saccorotti, G., Petrosino, S., Bianco, F., Castellano, M., Galluzzo, D., La Rocca, M., Del Pezzo, E.,
803 Zaccarelli, L., Cusano, P., 2007. Seismicity associated with the 2004–2006 renewed ground uplift at
804 Campi Flegrei caldera, Italy. Phys. Earth Planet. Inter. 165, 14–24. doi:10.1016/j. pepi.2007.07.006.

Sgattoni, G., Guðmundsson, Ó., Tryggvason, A., Lucchi, F., Einarsson, P., 2015. The 2011 unrest at Katla volcano: location and interpretation of the tremor source. Poster session presented at: 26th IUGG General Assembly 2015. Prague, Czech Republic.

Sigurðsson, O., Zóphoníasson, S., Ísleifsson, E., 2000. Jökulhlaup úr Sölheimajökli 18. júlí 1999 (The jökulhlaup from Sólheimajökull July 18, 1999, in Icelandic with English summary), Jökull 49, 75–80.

Soosalu, H., Jónsdóttir, K., Einarsson, P., 2006. Seismicity crisis at the Katla volcano, Iceland – signs of a cryptodome?. J. Volcanol. Geotherm. Res. 153, 177–186.

Spaans, K., Hreinsdóttir, S., Hooper, A., Ófeigsson, B.G., 2015. Crustal movements due to Iceland's shrinking ice caps mimic magma inflow signal at Katla volcano. Sci. Rep. 5, 10285. doi: 10.1038/srep10285

Sturkell, E., Einarsson, P., Sigmundsson, F., Geirsson, H., Ólafsson, H., Pedersen, R., de Zeeuw-van Dalfsen, E., Linde, A.T., Sacks, S.I., Stefánsson, R., 2006. Volcano geodesy and magma dynamics in Iceland. J. Volcanol. Geotherm. Res. 150, 14–34. doi:10.1016/j.jvolgeores.2005.07.010

Sturkell, E., Einarsson, P., Roberts, M.J., Geirsson, H., Guðmundsson, M.T., Sigmundsson, F., Pinel, V., Guðmundsson, G.B., Olafsson, H., Stefansson, R., 2008. Seismic and geodetic insights into magma accumulation at Katla subglacial volcano, Iceland: 1999 to 2005. J. Geophys. Res. 113, B03212.

Sturkell, E., Einarsson, P., Sigmundsson, F., Hooper, A., Ófeigsson, B. G., Geirsson, H., Ólafsson, H., 2010. Katla and Eyjafjallajökull Volcanoes. In: Schomacker, A., Krüger, J., Kjær, K.H. (Eds). The Mýrdalsjökull icecap, Iceland. Glacial processes, sediments and landforms on an active volcano. Developments in Quaternary Science 13. Elsevier, Amsterdam. ISBN 1571-0866, pp. 5–21.

Thelen, W. A., Allstadt, K., De Angelis, S., Malone, S. D., Moran, S. C., Vidale J., 2013. Shallow repeating seismic events under an alpine glacier at Mount Rainier, Washington, USA. J. Glaciol. 59, 214.

Thórarinsson, S., 1975. Katla og annáll Kötlugosa (Katla and its eruption history, in Icelandic). Árbók Ferðafélags Íslands. Ferðafélag Íslands, Reykjavík, 125-149.

829 Thordarson, T., Miller, D.J., Larsen, G., Self, S., Sigurðsson, H., 2001. New estimates of sulfur degassing
830 and atmospheric mass-loading by the 934 AD Eldgjá eruption, Iceland. J. Volcanol. Geotherm. Res.
831 108, 33–54.

832 Weaver, C. S., Malone, S. D., 1979. Seismic evidence for discrete glacier motion at the rock-ice interface. J.
833 Glaciol. 23, 171– 184.

834 West, M.E., Larsen, C.F., Truffer, M., O'Neel, S., LeBlanc, L., 2010. Glacier microseismicity. Geology, 38(4),
835 319–322. doi:10.1130/G30606.1

836 Wiens, D. A., Anandakrishnan, S., Winberry, J.P., King, M.A., 2008. Simultaneous teleseismic and geodetic
837 observations of the stick-slip motion of an Antarctic ice stream. Nature, 453, 770– 774.

838 Winberry, J.P., Conway, H., Huerta, A.D., Anandakrishnan, S., Aster, R.C., Koutnik, M., Nyblade, A.,
839 Wiens, D.A., 2015. Periodic, episodic, and complex behavior of glacial earthquakes. Paper presented
840 at: 26th IUGG General Assembly 2015. Prague, Czech Republic.

841 Wolf, B.Y.L.W., Davies, J.N., 1986. Glacier-generated earthquakes from Prince William Sound, Alaska.
842 Bull. Seismol. Soc. Am. 76, 367–379.

843